



OPEN ACCESS

EDITED BY

Jun Liu,
Yuebei People's Hospital, China

REVIEWED BY

Ganglei Li,
Zhejiang University, China
Yufeng Gao,
First Affiliated Hospital of Anhui
Medical University, China

*CORRESPONDENCE

Chengzeng Wang
czw202112@zzu.edu.cn
Lin Liu
liulin@zzu.edu.cn
Zhenqiang Sun
fccsunzq@zzu.edu.cn

[†]These authors have contributed
equally to this work

SPECIALTY SECTION

This article was submitted to
Cancer Immunity
and Immunotherapy,
a section of the journal
Frontiers in Immunology

RECEIVED 26 May 2022

ACCEPTED 28 June 2022

PUBLISHED 25 July 2022

CITATION

Dang Q, Liu Z, Liu Y, Wang W, Yuan W,
Sun Z, Liu L and Wang C (2022)
LncRNA profiles from Notch signaling:
Implications for clinical management
and tumor microenvironment of
colorectal cancer.
Front. Immunol. 13:953405.
doi: 10.3389/fimmu.2022.953405

COPYRIGHT

© 2022 Dang, Liu, Liu, Wang, Yuan, Sun,
Liu and Wang. This is an open-access
article distributed under the terms of
the [Creative Commons Attribution
License \(CC BY\)](https://creativecommons.org/licenses/by/4.0/). The use, distribution
or reproduction in other forums is
permitted, provided the original
author(s) and the copyright owner(s)
are credited and that the original
publication in this journal is cited, in
accordance with accepted academic
practice. No use, distribution or
reproduction is permitted which does
not comply with these terms.

LncRNA profiles from Notch signaling: Implications for clinical management and tumor microenvironment of colorectal cancer

Qin Dang^{1,2†}, Zaoqu Liu^{3†}, Yang Liu^{4†}, Wenkang Wang⁵,
Weitang Yuan¹, Zhenqiang Sun^{1,2*}, Lin Liu^{2,6*}
and Chengzeng Wang^{2,6*}

¹Department of Colorectal Surgery, The First Affiliated Hospital of Zhengzhou University, Zhengzhou, China, ²Henan Institute of Interconnected Intelligent Health Management, The First Affiliated Hospital of Zhengzhou University, Zhengzhou, China, ³Department of Interventional Radiology, The First Affiliated Hospital of Zhengzhou University, Zhengzhou, China, ⁴Department of Radiotherapy, Affiliated Cancer Hospital of Zhengzhou University, Henan Cancer Hospital, Zhengzhou, China, ⁵Department of Breast Surgery, The First Affiliated Hospital of Zhengzhou University, Zhengzhou, China, ⁶Department of Ultrasound, The First Affiliated Hospital of Zhengzhou University, Zhengzhou, China

The interplay between long non-coding RNAs (lncRNAs) and the Notch pathway involves a variety of malignancies. However, Notch-derived lncRNAs and their latent clinical significance remain elusive in colorectal cancer (CRC). In this study, we introduced a framework that could screen Notch-derived lncRNAs (named "NLncr") and ultimately identified 24 NLncers. To further explore the clinical significance of these NLncers, we performed LASSO and Cox regression in TCGA-CRC cohort (n = 584) and then retained six lncRNAs tightly associated with prognosis. The final model (termed "NLncS") was subsequently tested in GSE38832 (n = 122), GSE39582 (n = 573), and an in-house clinical cohort (n = 115). Ultimately, our NLncS model could serve as an independent risk factor and afford a robust performance for assessing the prognosis of CRC patients. Additionally, patients with high NLncS risk scores were characterized by upregulation of immune pathways, strong immunogenicity, abundant CD8 + T-cell infiltration, and potentially higher response rates to CTLA4 blockers, which turned out to be suitable for immunotherapy. Aiming at globally observing the characteristics of high-risk patients, somatic mutation and methylation modification analysis provide us with evidence at the genomic and transcriptomic levels. To facilitate the clinical transformability, we mined deeply into the sensitive compounds targeting high-risk individuals and identified dasatinib as a candidate agent for patients with a high Notch risk score. In conclusion, our NLncS model is a promising biomarker for optimizing the clinical management of CRC patients.

KEYWORDS

colorectal cancer, LncRNA, notch, prognosis, immunotherapy, tumor microenvironment

Introduction

As one of the primary causes in tumor-related death, colorectal cancer (CRC) ranks the third most common malignant neoplasm worldwide (1, 2). CRC is often diagnosed at an advanced stage, accompanied by high postoperative recurrence and metastasis rate, which seriously threatens the health of the public. The survival of CRC patients was subjected to a series of clinical difficulties such as unresectable surgery, chemotherapy resistance, and radiotherapy side effects (3, 4). Notably, immunotherapy has shown spectacular achievements in the oncology treatment field (5, 6). However, with the rapid development, limitations of immunotherapy emerged. As proof, immunotherapy brings the desired curative effect when applied to the suitable patient subgroups (7, 8). To address this plight, researchers need to precisely identify individuals suitable for immunotherapy.

The Notch pathway, a signal transduction system ubiquitous in cellular organisms, determines the cell fate and function (9). Studies widely validated that the Notch pathway is involved in diversified aspects of oncology, including carcinogenesis, metastasis, stemness, metabolism, apoptosis, and angiogenesis (10–15). *NOTCH3* expression is closely associated with malignant phenotypes of CRC, including higher grade, the existence of lymph nodes, and distant metastasis (10). Additionally, several Notch signaling receptors could serve as therapeutic targets for breast cancer (16). Moreover, accumulating evidence has shown that the Notch pathway influences the immune system, both innate and adaptive, *via* dendritic cells and T cells (17, 18).

For decades, the identification of abundant long non-coding RNAs (lncRNAs) >200 bp has brought out their characterization as profound components in tumor biology. lncRNA molecules were commonly present in tumors as a double-edged sword of driving tumor development or inhibiting progression (19–22). Previous studies have confirmed that lncRNA could govern key ligands in the Notch pathway to achieve tumor control, such as breast cancer, renal cell cancer, and gastric cancer (23–25). Nevertheless, the comprehensive landscape of the Notch pathway-related lncRNA in CRC remains elusive, and we hope to endue Notch pathways with a novel character and clinical application through functional lncRNA analysis.

Herein, we constructed an integrated frame capable of identifying Notch-derived lncRNA drivers (termed “NLncr”). We characterized the prognostic value of the Notch-related lncRNA signature (NLncS) for CRC patients and distinguished high-risk subgroups that are suitable for immunotherapy. For verification, two independent cohorts and a clinical in-house dataset were enrolled. Subsequently, we probed the methylation levels of distinct individuals in order to find genome-level drivers that contribute to differences in outcomes. Further, based on cell

line expression profiles and drug sensitivity results (CTRP and PRISM) and Connectivity Map (CMap) analysis, we recommend the anticancer drug dasatinib as a latent treatment for a CRC high-risk subgroup.

Materials and methods

Public dataset collection and procession

The workflow of this research is depicted in Figure 1. A total of 1,279 CRC patients from three independent public cohorts were obtained from The Cancer Genome Atlas (TCGA, <https://portal.gdc.cancer.gov>) and Gene Expression Omnibus (GEO, <http://www.ncbi.nlm.nih.gov/geo>), including TCGA-CRC, GSE39582, and GSE38832 (Supplementary Table 1). We transformed the RNA-seq raw read count of TCGA-CRC to transcripts per kilobase million (TPM). The GEO datasets were collected from the Affymetrix® Human Genome U133 Plus 2.0 Array (GPL570 platform) and processed by the robust multiarray averaging (RMA) algorithm with the *Affy* package. We obtained 19,526 protein-coding genes and 15,299 lncRNAs from TCGA database based on GENCODE (Homo sapiens GRCh38, <https://www.encodegenes.org/>). All probes were mapped to the human genome (Hg38), and 3,439 lncRNAs were acquired by reannotating the probe sets of the GPL570 array (26). Given the batch effect, we combined the colonic adenocarcinoma (COAD) and rectum adenocarcinoma (READ) data into TCGA-CRC queues after *ComBat* algorithm-based processing. lncRNAs with an empty expression in more than half of the sample size in each cohort were excluded. Detailed baselines for three independent queues are pooled in Supplementary Table 1.

NLncr: screening the potential lncRNA drivers of the Notch pathway

Aiming at discovering potential Notch-associated lncRNA drivers, we developed a comprehensive pipeline by referring to previous findings (27, 28). In brief, we arranged the mRNAs in descending order to the pertinence of particular lncRNA adjusted for tumor purity. The *fgsea* R package was used to determine whether Notch pathway-related genes were enriched. Next, the Notch enrichment score (NES) of all lncRNAs was measured, and those with significant NES were identified as NLncers. lncRNA *i* and mRNA *k* in *n* samples were termed as $Lnc(i) = (lnc_1, lnc_2, \dots, lnc_n)$ and $M(k) = (m_1, m_2, \dots, m_n)$ in the expression matrix, respectively. The tumor purity of *n* patients was quantified *via* the *ESTIMATE* R package and termed as p_1, p_2, \dots, p_n . The first-order partial correlation coefficients (PCCs) of lncRNA *i* and mRNA *k* were determined by performing the following operation:

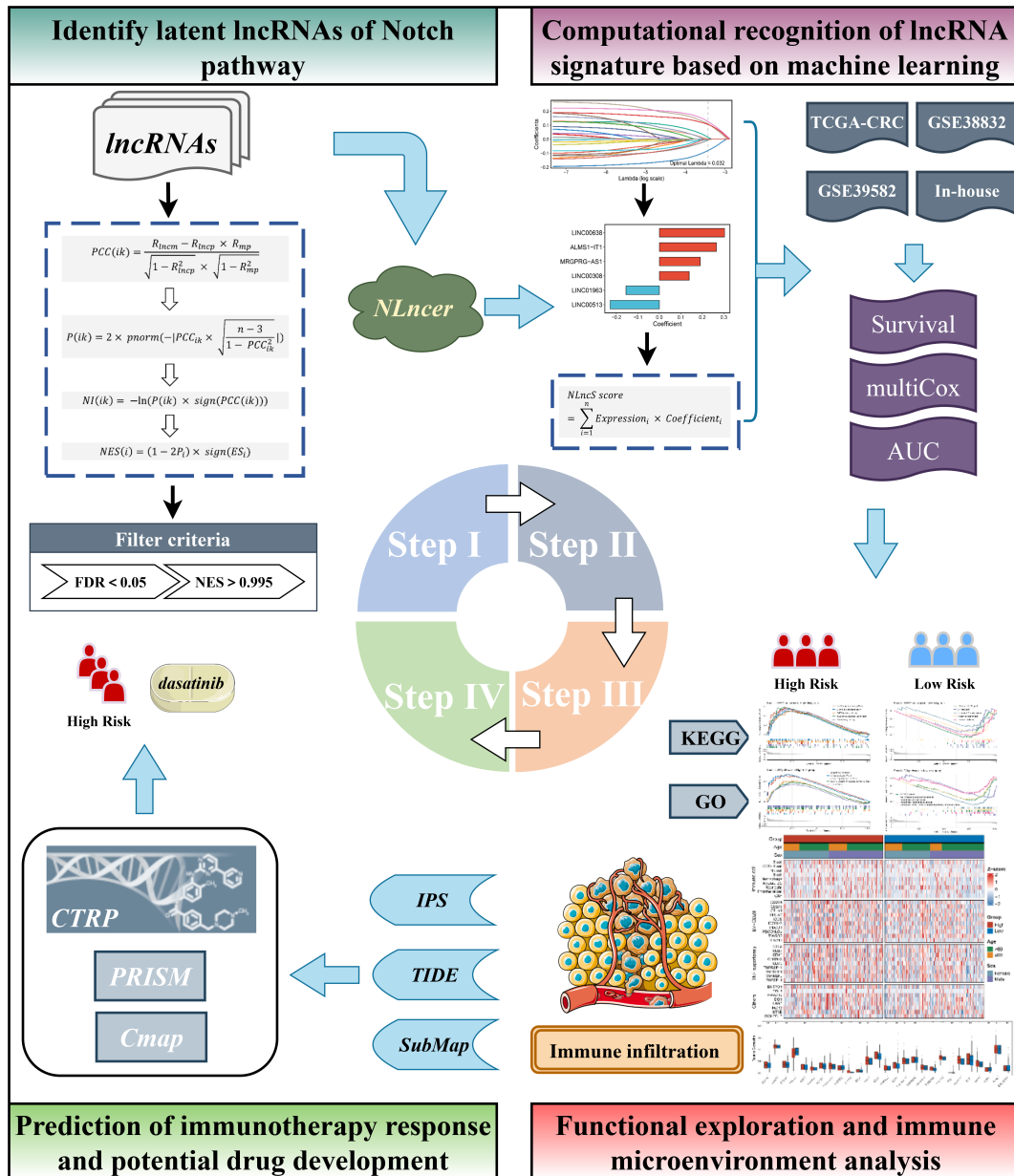


FIGURE 1
The workflow of the study.

$$PCC(ik) = \frac{R_{lncm} - R_{lncp} \times R_{mp}}{\sqrt{1 - R_{lncp}^2} \times \sqrt{1 - R_{mp}^2}}$$

R_{lncm} , R_{lncp} , and R_{mp} were named as the Pearson correlation coefficients of lncRNA i and mRNA k , lncRNA i and tumor purity p , and mRNA k and tumor purity p , respectively. Then, $P(i|k)$, the P -value of $PCC(ik)$, was calculated:

$$P(i|k) = 2 \times pnorm\left(-|PCC_{ik}| \times \sqrt{\frac{n-3}{1 - PCC_{ik}^2}}\right)$$

$pnorm$ is defined as the normal distribution function, and n is the sample size. The Notch index (NI) was measured:

$$NI(ik) = -\ln(P(i|k) \times \text{sign}(PCC(ik)))$$

sign is a method that could realize the symbolic separation of functions. All mRNAs were sequenced according to descending *NI*, and further gene set concentration analysis (GSEA) was performed. The adjusted *P*-values and concentration scores (*ES*) of lncRNA *i* were evaluated by the *fgsea* R package and combined into a *NES*:

$$NES(i) = (1 - 2P_i) \times sign(ES_i)$$

Thereby, the *NES* was calculated to range from -1 to 1. Referring to previous findings (27, 28), lncRNAs with false discovery rate (FDR) <0.05 and *NES* absolute value >0.995 were filtrated as Notch-derived lncRNAs.

Signature generation

Given the comparability between disparate cohorts, lncRNA expression in three cohorts was converted to z-score before Notch-related lncRNA signatures (NLncS) were generated. According to the expression profile of Notch-derived lncRNAs, univariate Cox regression was calculated among TCGA-CRC, GSE39582, and GSE38832. Aware that the rigor of multiple test corrections and the small sample size may screen out some latent lncRNAs associated with survival, lncRNAs with unadjusted *P* < 0.15 and the same hazard ratio (HR) direction were adopted to construct the NLncS in combination with LASSO regression (29). The optimal lambda was obtained when the partial likelihood deviation achieved the minimum by adopting the 10-fold cross-validation algorithm. The lncRNAs with non-zero coefficients were involved in fitting signatures. The NLncS equation was computed with the following LASSO model weighting coefficient:

$$NLncS\ score = \sum_{i=1}^n Expression_i \times Coefficient_i$$

n refers to the total of significant lncRNAs, *Expression_i* stands for the lncRNA *i* expression, and *Coefficient_i* replaced the matching regression coefficient.

Clinical specimens and information collection

The ethics committee of the First Affiliated Hospital of Zhengzhou University provided consent to the study. One hundred fifteen pairs of CRC primary and normal tissues surgically resected in the First Affiliated Hospital of Zhengzhou University were included. The patient selection criteria were as follows: 1) no preoperative treatment, such as radiotherapy, chemotherapy, or targeted therapy was received; 2) no complication of any other tumors; 3) no autoimmune disease. [Supplementary Table 1](#) provides the record of the baseline data. Fresh specimens were obtained and frozen in

liquid nitrogen at -80°C for preservation. The clinical stage was in accordance with NCCN (2019) guidelines. Each individual signed informed consent. The relevant ethical review number is 2019-KY-423.

Quantitative real-time PCR

Tissue RNA was extracted by RNAiso Plus (Takara, China) reagent, and the quality was evaluated by NanoDrop One C (Waltham, USA). Complementary DNA (cDNA) was obtained by following the protocol of the Reverse Transcription Kit (Takara Bio, Japan). Then, quantitative real-time polymerase chain reaction (qRT-PCR) was performed using SYBR Assay I Low ROX (Eurogentec, USA) and SYBR[®] Green PCR Master Mix (Yeason, China). Each test was repeated three times. The expression level was quantized by 2^{-ΔΔCt} mode. GAPDH serves as an internal reference for normalization. The reader is referred to [Supplementary Table 2](#) for primer sequence information.

Functional enrichment

For distinguishing the differences of distinct NLncS scores, the GSEA tool and *clusterProfiler* package were used to analyze the biological pathways of Kyoto Encyclopedia of Genes and Genomes (KEGG) and Gene Ontology (GO) (30). To get a standardized concentration, we chose the permutation to 1,000. Gene sets with adjusted *P*-value <0.05 were selected as significant.

Immune infiltration assessment

We adopted the *MCPcounter* package to explore immune cell type, stromal cell, and immune checkpoint (ICPs, recruited *B7-CD28* family, *TNF superfamily*, and others, [Supplementary Table 5](#)) abundance in CRC tissues (31). The correlation between these immune components and the NLncS model was further compared.

The mutation landscape and copy number variation of CRC

Somatic mutation and copy number variation (CNV) data were downloaded from TCGA-CRC portal and cBioportal website, respectively. The *TCGAbiolinks* R package was performed to get the raw mutation file. Mutations in different patient subpopulations were analyzed and visualized based on the *maftools* and *ComplexHeatmap* R package. CNV waterfall maps of the first 10 amplification (AMP) and homozygous

deletion (Homdel) chromosome fragments were visualized by the *ComplexHeatmap* package.

Estimation of methylation drivers

The raw methylation data were obtained from HumanMethylation450 array TCGA-CRC. The global methylation level (GML) of each TCGA-CRC sample was quantified based on the average beta value of a particular probe (32). The *MethylMix* package was adopted for integration of methylation and mRNA expression data. Methylation drivers, genes that were considerably inversely correlated with expression, were used to investigate the association with NLncS.

Evaluation of response to immunotherapy

Combining the immunophenoscore (IPS), tumor immune dysfunction and exclusion (TIDE, <http://tide.dfci.harvard.edu/>), and subclass mapping (SubMap) algorithms predicts responsiveness to immunotherapy (33–35). TIDE is an algorithm that integrates T-cell features to characterize immune evasion situations. The IPS Z-score was computed by assessing the scores of four immunophenotypes (antigenic presentation, effector cell, inhibitory cell, and ICP) (36). The higher IPS foreboded stronger immunogenicity of individuals. SubMap was adopted to judge the degree of similarity. The Bonferroni-corrected *P* was applied to indicate similarity, and the magnitude of the *P*-value is negatively correlated with similarity.

Prediction of therapeutic agents

The Cancer Therapeutics Response Portal datasets (CTRP) and PRISM databases store cancer cell line (CCL) sensitivity data with over 481 and 1448 compounds, respectively. In addition, both data provide the area under the curve (AUC) of dose-response as a measure of drug sensitivity. A lower AUC predicts stronger drug responsiveness. After filtering out compounds with $\geq 20\%$ missing AUC values, the K-nearest neighbor (k-NN) imputation method was employed to interpolate missing variables for the remaining compounds.

Alternative compounds that target with high-risk groups

CMap (<https://portals.broadinstitute.org/cmap/>), a public online tool developed from the Broad Institute, was used to

determine which drugs may have an effect on high-risk samples (37). Differential expression genes (DEGs) were obtained *via* the *limma* package. Subsequently, the top 150 upregulated and 150 downregulated genes were selected for CMap analysis. Each ranked list in CMap datasets was compared with DEGs to specify where the DEGs appeared, thus yielding a score of -100 to 100. Then the enrichment score was re-ranked; the top is strongly and positively correlated with the high risk, and the bottom is the opposite.

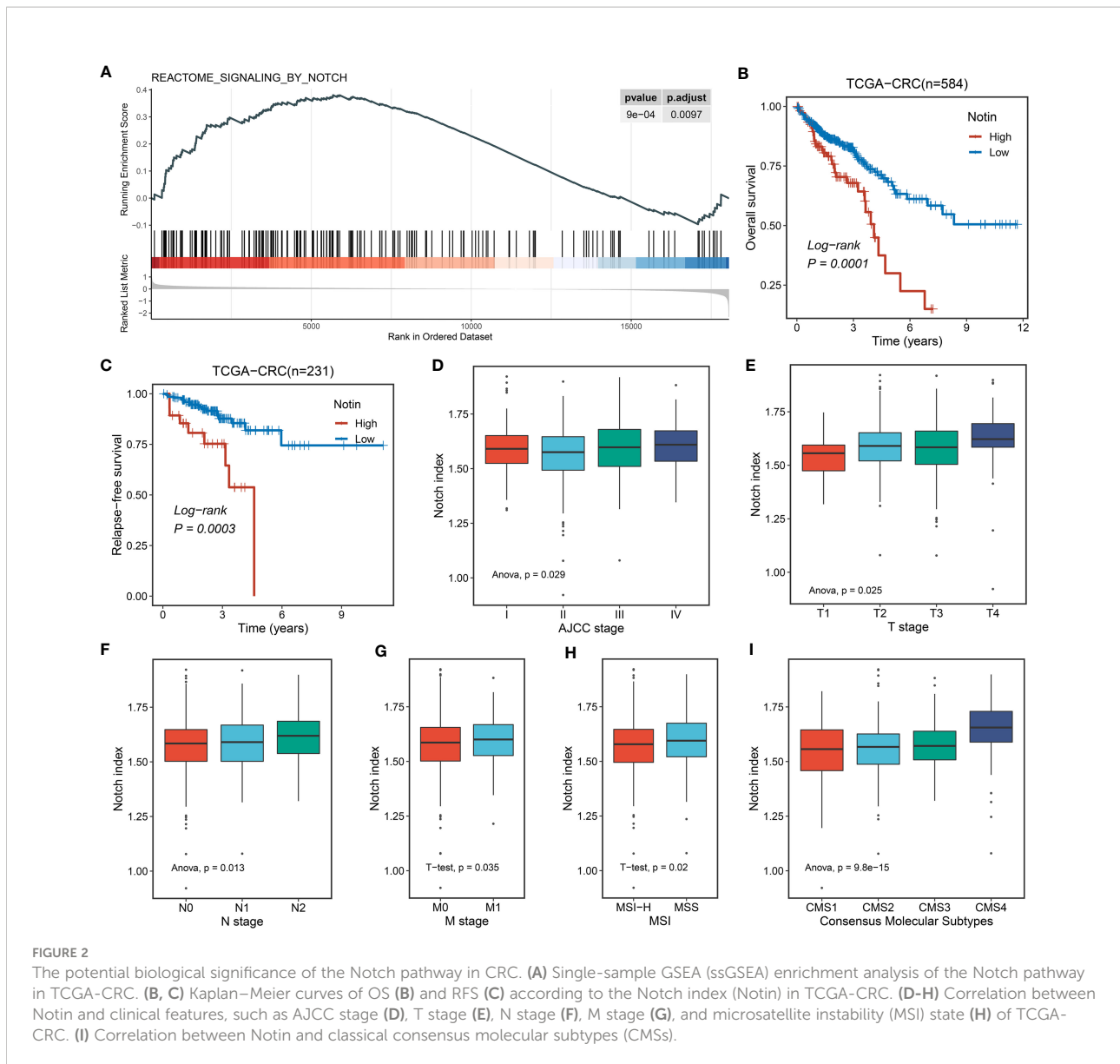
Statistical analysis

All work was performed in R software (4.1.0). Pearson's chi-square test was used for categorical variables. Continuous variables were compared adapting the Wilcoxon rank-sum test or Student's *t* test. Spearman analysis was used to analyze the correlation between groups. The *glmnet* package was adopted to fit LASSO regression. Cox regression and Kaplan–Meier (K-M) analysis were computed based on the *survival* package. The optimal cutoff value was chosen by the *survminer* package. Survival ROC and AUC were quantified *via* the *timeROC* package. *P* < 0.05 of two tails was judged statistically significant.

Results

The Notch pathway was significantly enriched and correlated with clinical features of CRC

For decades, the functional impact of the Notch pathway-based interplay with lncRNAs for neoplastic diseases has gradually become the focus of researchers' attention. In this context, we proposed whether a Notch pathway-derived global lncRNA signature could improve the outcomes and treatment efficacy and seek potential drugs for CRC patients. To address the question, we initially validated the Notch index of CRC primary and normal tissues in TCGA-CRC (for training dataset) cohort. Accordingly, the Notch signaling pathway was upregulated in tumor tissues (Figure 2A). Further, we utilized single-sample GSEA (ssGSEA) to evaluate the index of Notch pathway features for each sample. K-M analysis showed that the high Notch index predicted the adverse overall survival (OS, log-rank *P* = 0.0001) and relapse-free survival (RFS, log-rank *P* = 0.0003) of patients (Figures 2B, C). In addition, correlation analysis between the Notch index and clinical features showed that a high Notch index tended to be associated with a high clinical stage (such as AJCC stage, T, N, and M stage) and microsatellite stability (all *P* < 0.05, Figures 2D–H). Notably, the establishment of consensus molecular subtypes (CMSs) provides the most reliable classification system for CRC to date (38). We further explored the underlying link between the Notch index



and CMS1–4 and found that CMS4 (mesenchymal subtype) had the highest Notch index ($P < 0.001$, Figure 2I). The CMS4 subtype prominently manifested an upregulation of epithelial–mesenchymal transition, angiogenesis, and lowest survival. Collectively, the above support that the Notch pathway has profound predictive value in CRC.

Nlncr to NLncS: Identifying Notch-derived LncRNA and generating a signature with the LASSO algorithm

For better consistency, we retained a total of 3,390 lncRNA molecules with relevant data in the three cohorts. Based on our previously developed framework of “TGFmitor” and the

recognition of an immune-related lncRNA signature, similarly, we screened and obtained 24 candidate lncRNAs stably associated with the Notch pathway (27, 39, 40). According to the expression profiles of these 24 lncRNAs, we constructed the LASSO model *via* a 10-fold cross-validation. When the optimal lambda of 0.032 was selected, eight key lncRNA molecules with non-zero coefficients were identified (Figure 3A). Subsequently, after multivariate Cox regression, six lncRNAs stably associated with OS were used to construct the model, namely, LINC00638, ALMS1-IT1, MRGPRG-AS1, LINC00308, LINC01963, and LINC00513 (Figure 3B). Finally, a continuous risk score of the NLncS model was computed through a linear combination of regression coefficient-weighted expression values of the six lncRNAs. Next, we distinguish the high- and low-risk samples according to the median value. In TCGA-CRC, GSE38832, and

GSE39582, the high-risk group presented a prominently worse prognosis than the low-risk group (all Log-rank $P < 0.0001$, Figures 3C, D, F). After incorporating available clinical characteristics including age, sex, stage (T, N, M, and AJCC), and microsatellite instability (MSI) state, multivariate Cox regression showed that NLncS were still statistically significant. This suggests that NLncS can be used as an independent prognostic factor for CRC (all $P < 0.001$, Figures 3E, G, Supplementary Figure 1A). We detected the recognition of NLncS and calculated the AUC at 1, 3, and 5 years of TCGA-CRC (0.780, 0.780, and 0.806), GSE38832 (0.701, 0.762, and 0.768), and GSE39582 (0.701, 0.762, and 0.768). We compared the NLncS model with three other lncRNA signatures. It was found that our NLncS model had the highest C-index and was significantly better than the other three lncRNA prediction models ($*P < 0.05$, $***P < 0.0001$, Supplementary Figure 3, Supplementary Table 4) (41–43). Therefore, NLncS possessed the ability of robust prediction in CRC patients.

Clinical in-house cohort for NLncS validation via qRT-PCR

To further explore the potential for clinical translational applications of NLncS, we examined the expression of lncRNAs via qRT-PCR and calculated risk scores in a clinical in-house cohort. The results are plotted in Figure 4. Patients with high-risk scores had lower OS (Figure 4A) and disease-free survival (DFS, Figure 4B), which validates the prognostic predictive power of the model ($P < 0.0001$ for both). After inclusion of clinical and pathological features, multivariate analysis showed that risk score was an independent indicator in both OS (Figure 4C, $P < 0.001$) and DFS (Figure 4D, $P = 0.006$). What is more, the AUC calculation of the model showed that the 1-, 3-, and 5-year AUC values were 0.703, 0.916, and 0.837 for OS and 0.674, 0.911, and 0.770 for DFS (Figures 4E, F), respectively, showing good predictive power.

Immune-related mechanisms were upregulated in the high-risk group, showing potential immunologic properties

Further, we performed GSEA to explore the potential biological mechanisms that may cause differences on two groups. We found a significant enrichment of signaling pathways in the high-risk group such as immunity (humoral and cellular immunity) and regulation of cellular differentiation (Figures 5A, C), for instance, B-cell receptor and chemokine signaling, T-cell activation and phagocytosis, and cellular differentiation-related pathways such as the MAPK pathway. However, the downregulation of energy metabolism and redox

reactions was predominantly related with the low-risk group, including glycolysis, tricarboxylic acid cycle (TCA cycle), aerobic respiration, and oxidative phosphorylation (Figures 5B, D). Hence, it is manifest that immune-related roles may be influencing factors contributing to NLncS predicting differences.

Tumor immune microenvironment landscape and immune checkpoint profiles of NLncS

Since immune-related pathways differ among subgroups of NLncS, we expanded our analysis of the tumor immune microenvironment (TIME) landscape consisting of nine immune cell types and 27 immune checkpoints to further distinguish immune features. The scenario is depicted in Figure 5E. Moreover, CD8+ T cells, macrophages, endothelial cells, and cancer-associated fibroblasts (CAFs) were significantly enriched in the high-risk group (Supplementary Figure 1B). Specifically, HHLA2 was overexpressed in the low-risk group, while ICOSLG, PDCD1, PDCD1LG2, VTCN1, CD40, TNFRSF9, TNFSF14, ENTPD1, HAVCR2, and LAG3 were considerably overexpressed in the high-risk group (Figure 5F). Thus viewed, both at the level of pathway enrichment, cell infiltration, and molecular expression, the high- and low-risk groups showed more or less imparities.

Somatic mutation landscape, CNVs, and latent methylation driver in CRC

Previously, it has been reported that tumors with a high mutation load were more likely to respond to clinical strategies based on immune checkpoint blockers (44–47). Indeed, based on the immunological background of NLncS, we next estimated the effects of somatic mutation on NLncS for seeking clinical benefit. Figure 6A depicts the mutational landscape of NLncS. APC and TP53 ranked first and second with 79% and 61% mutation frequencies, respectively, which supported that high mutation rates of APC and TP53 might be responsible for giving rise to CRC (Figure 6A). Given that CNV dominantly consisted of amplification (AMP) and homozygous deletion (HOMDEL), we sequenced the genes by frequency of AMP and HOMDEL (Figure 6B). The results revealed that in the high-risk group, TTPAL, RAE1, R3HDML, PABPC1L, LINC01620, and LINC01430 were visibly amplified; dramatically deletions were RBFOX1, WWOX, and MACROD2. Interestingly, there was merely a slight difference in HOMDEL of the low-risk group. Visible amplifications were TTLL9, TM9SF4, POFUT1, PDRG1, MYLK2, and FOXS1.

Considering that the methylation modifications could alter the biological function of RNA molecules at the epigenetic stage, we performed a global methylation overview of CRC (48, 49). With the help of the *MethylMix* R package and Wilcoxon test, we found six

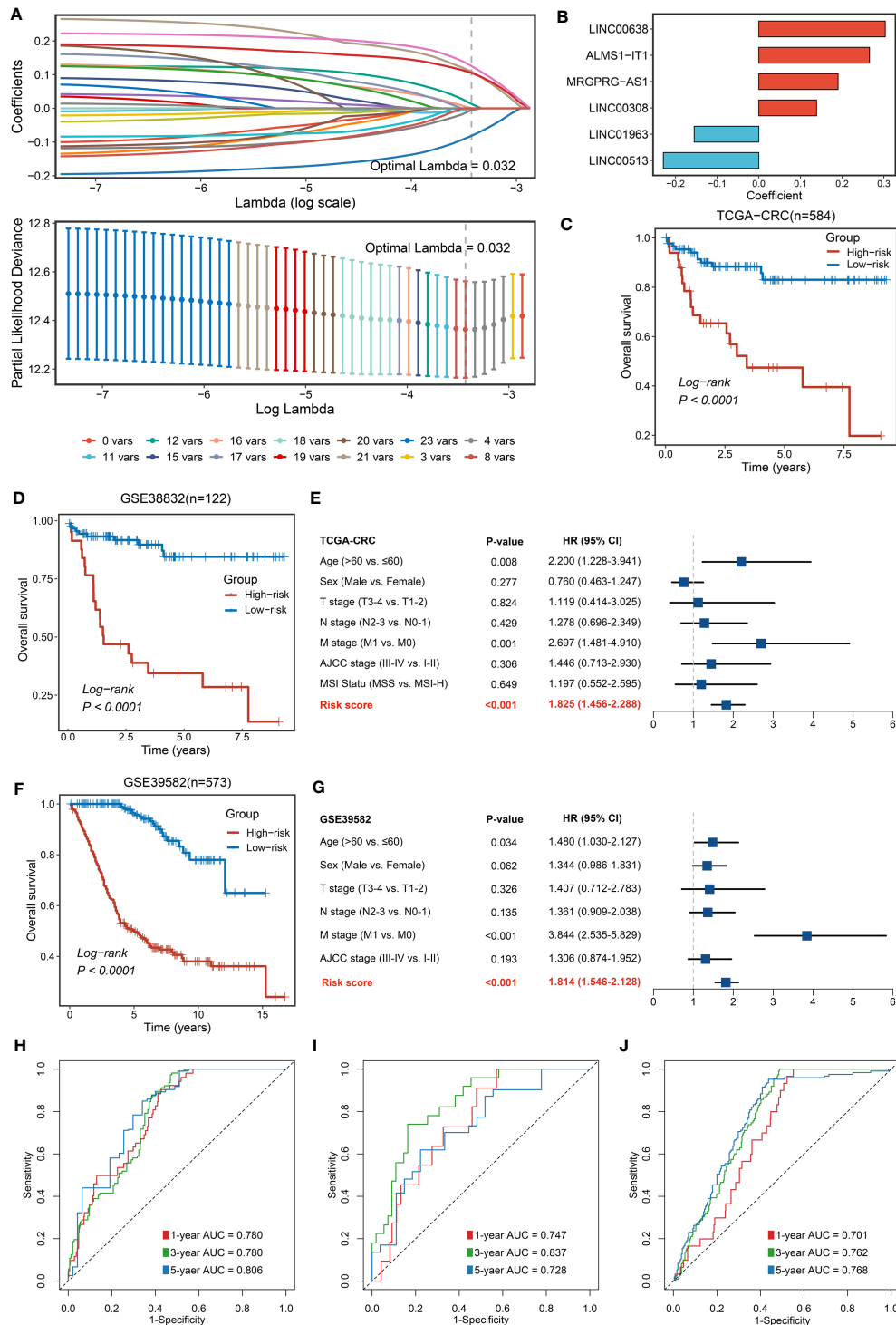


FIGURE 3

Construction and validation of NLncS. (A) Determination of the optimal lambda was obtained when the partial likelihood deviance reached the minimum value. (B) Univariate Cox regression was further performed to generate the key lncRNAs with non-zero coefficients and predictive values. LASSO coefficient profiles of the candidate lncRNAs for NLncS construction. (C, D, F) Kaplan–Meier curves of OS according to NLncS in TCGA-CRC (C), GSE38832 (D), and GSE39582 (F). (E, G) Multivariable Cox regression analysis of NLncS in TCGA-CRC (E) and GSE39582 (G). (H–J) Time-dependent ROC analysis for predicting OS at 1, 3, and 5 years in TCGA-CRC (H), GSE38832 (I), and GSE39582 (J).

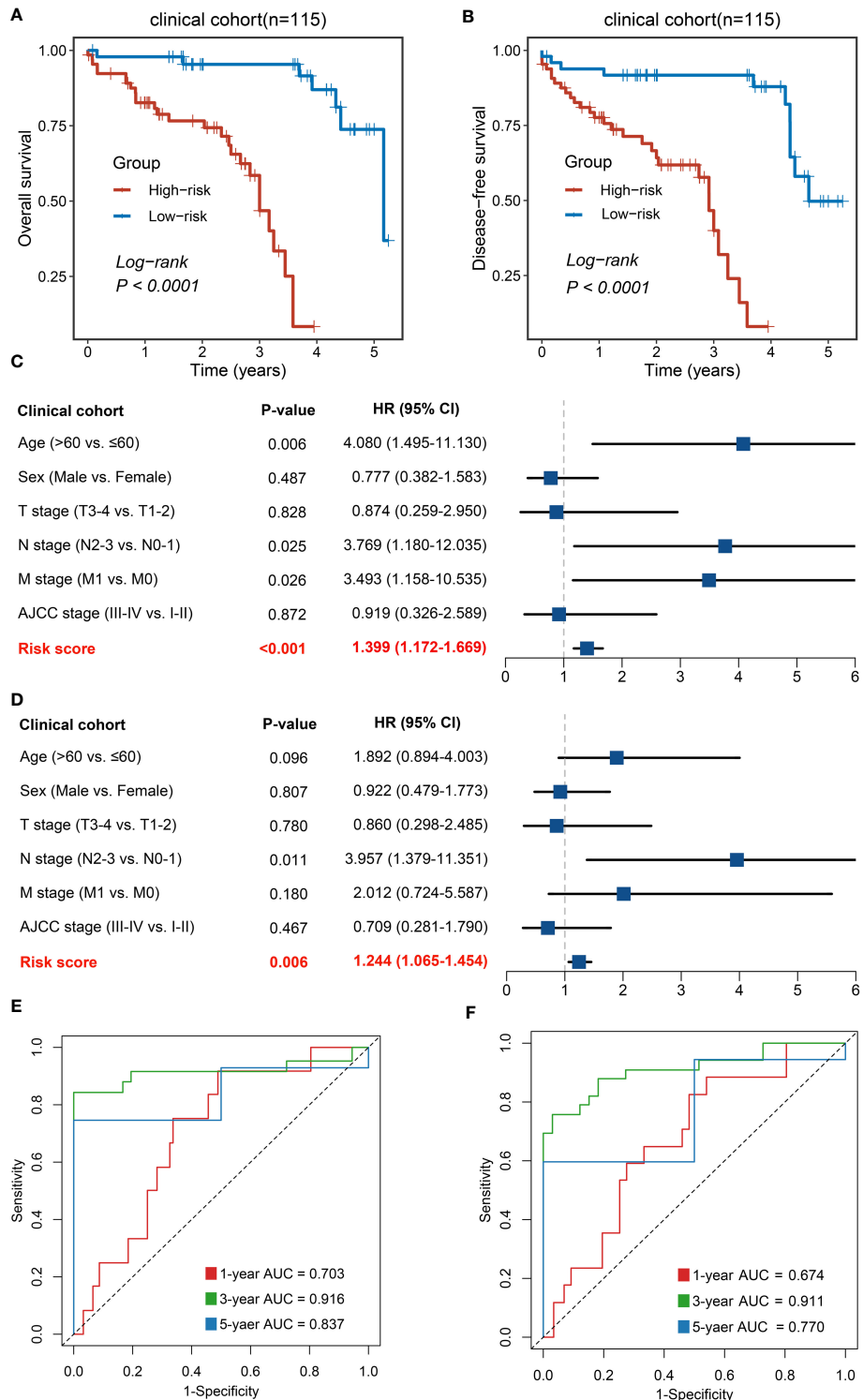


FIGURE 4 Validation of NLncS via qRT-PCR. (A, B) Kaplan–Meier curves of OS (A) and DFS (B) based on NLncS. (C, D) Multivariable Cox regression analysis of OS (C) and DFS (D). (E, F) Time-dependent ROC analysis for predicting OS (E) and DFS (F) at 1, 3, and 5 years.

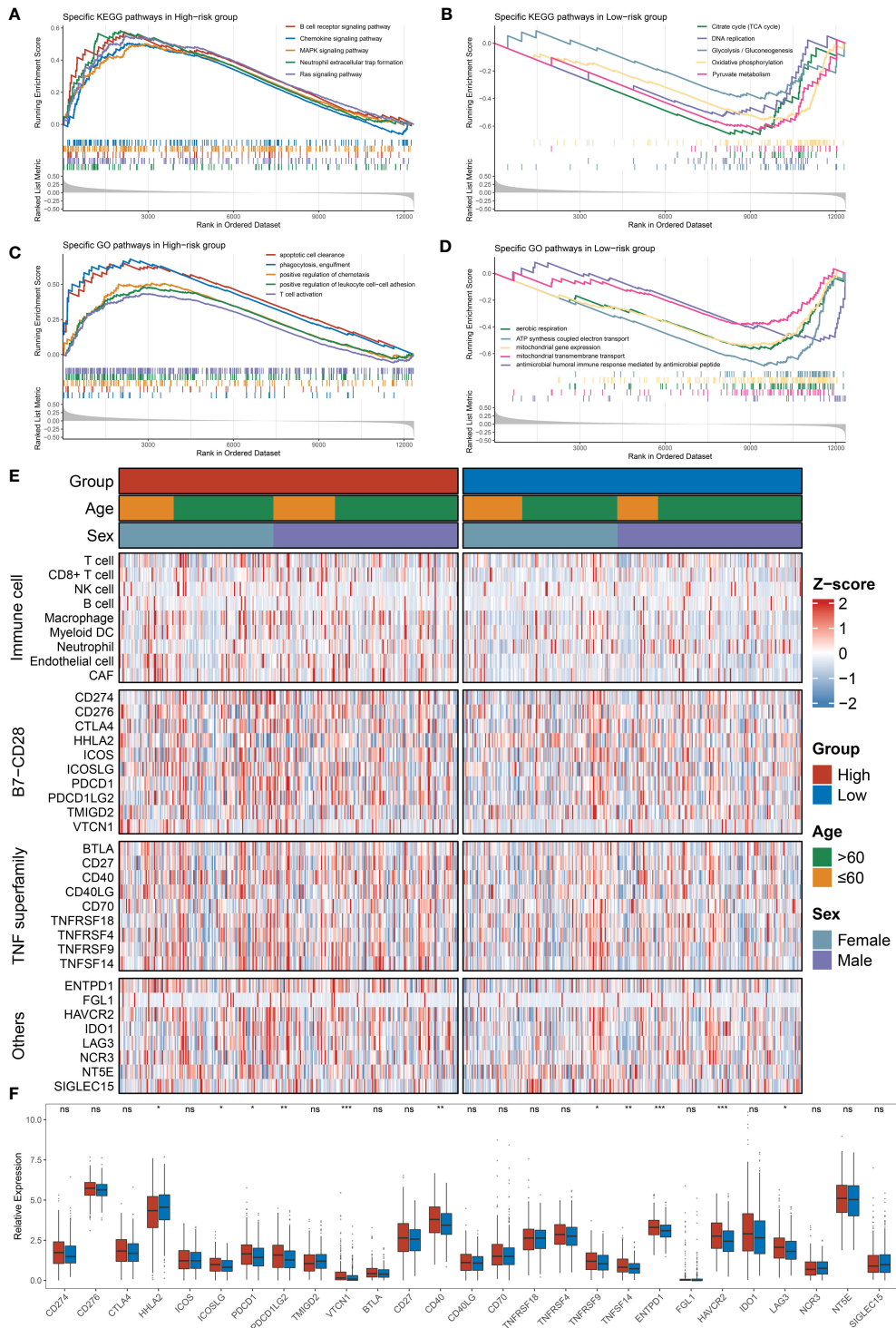


FIGURE 5 Functional enrichment analysis and immune infiltration analysis were performed in high- and low-risk groups. **(A, B)** The top five KEGG-enriched pathways and immune landscapes in the high- and low-risk groups. **(C, D)** The top five GO-enriched pathways and immune landscapes in the high- and low-risk groups. **(E)** The heatmaps of eight immune cell and 27 immune checkpoint profiles in the high- and low-risk groups. **(F)** The relative expression of 27 immune checkpoints in the high- and low-risk groups. (ns, none significance, $P > 0.05$; * $P < 0.05$; ** $P < 0.01$; *** $P < 0.001$).

methylation driver genes whose methylation levels were significantly negatively correlated with expression in two groups, including CES3, FAM127B, MAP9, PARVB, RLN2, and ZNF548. Strikingly, the growing NLncS fraction was accompanied by

increased methylation levels of CES3 and RLN2 but decreased expression levels (Supplementary Figure 2; Figures 6C, D). This suggested that CES3 and RLN2 might play an antitumor role as protective factors in the high-risk group, while methylation

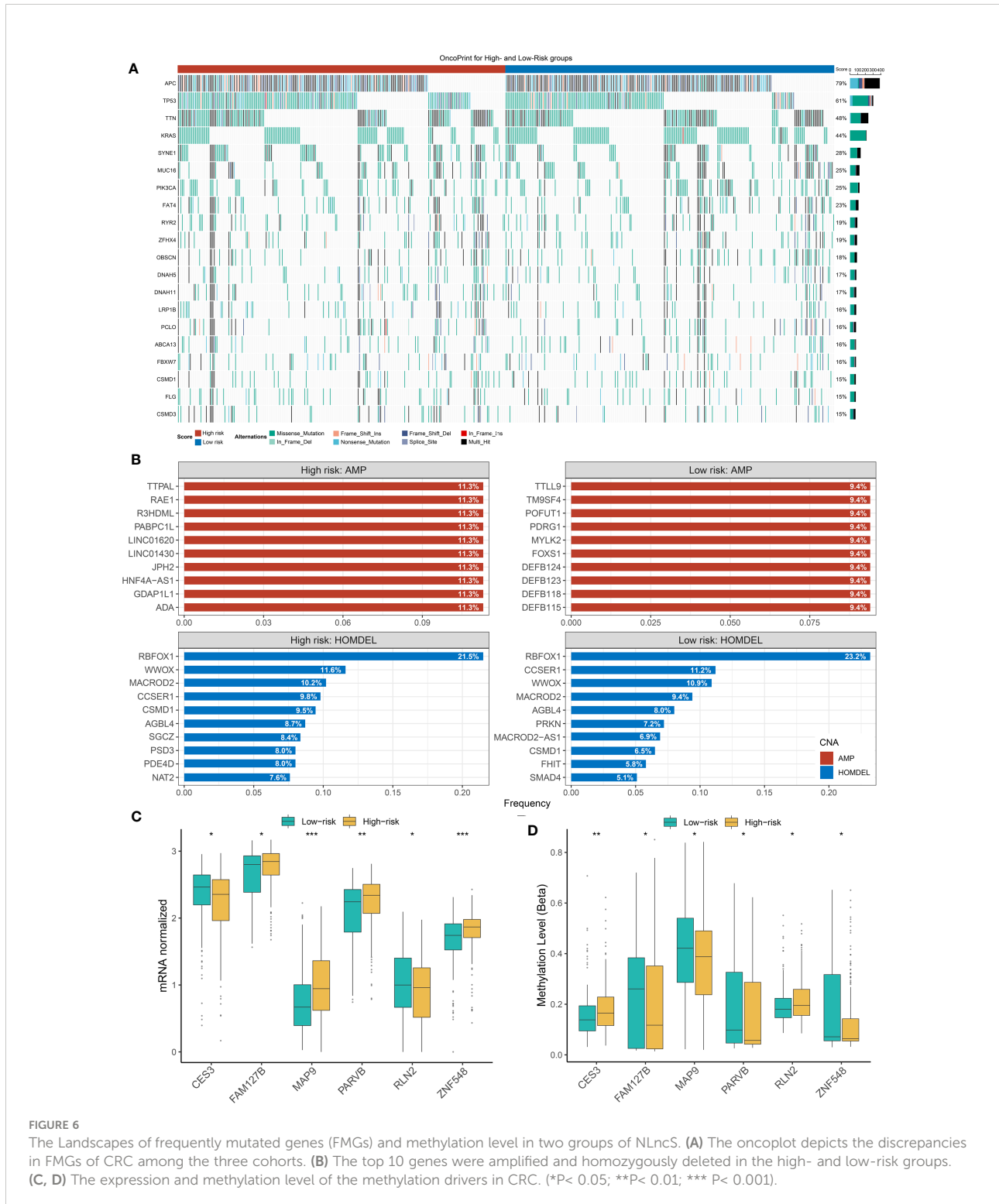


FIGURE 6

The Landscapes of frequently mutated genes (FMGs) and methylation level in two groups of NLncS. (A) The oncoPrint depicts the discrepancies in FMGs of CRC among the three cohorts. (B) The top 10 genes were amplified and homozygously deleted in the high- and low-risk groups. (C, D) The expression and methylation level of the methylation drivers in CRC. (*P < 0.05; **P < 0.01; *** P < 0.001).

modification silenced the corresponding mRNA fragments resulting in CES3 and RLN2 reduced expression levels. Collectively, this suggested that the influence of mutational burden, CNV, and methylation level on NLncS scores was likely non-redundant.

Deducing response to immunotherapy

As we all predicted, immunogenicity predicts stimulation to the immune system (50). As an evaluation tool of tumor immunogenicity, IPS was adopted to indirectly judge the local immune activation status of the sample. Scores were calculated for four different immunophenotypes (antigen presentation, effector cells, suppressor cells, checkpoints). The Z-score was the integration of the four. As expected, we found a significantly high Z-score in high-risk patients, indicating greater immunogenicity ($P < 0.0001$, Figure 7A). Guided by the TIDE network tool, the response rate to immunotherapy (50.7%) of the high-risk group was markedly higher ($P = 0.001$, Figure 7B). Further, according to the SubMap method, we compared the similarity in mRNA expression patterns between two groups of CRC patients and 47 patients who responded (R) or did not respond (NR) to immunotherapy. The result showed that high-risk patients were closer to those who responded to immunotherapy (Bonferroni corrected $P = 0.032$, Figure 7C). These results strongly indicate that high-risk individuals could benefit from immunotherapy.

Exploring insidious therapeutic agents for high-risk CRC individuals

Herein, referring to the workflow of Yang et al., we mined optional drugs for high-risk patients following the framework shown in Figure 7D (51). In order to obtain robust therapeutic drugs, we used two databases that store gene expression profile data and drug sensitivity data for CCLs, CTRP, and PRISM. After removing drugs with >20% missing values, we obtained 266 and 1285 compounds from CTRP and PRISM, respectively. We selected ridge regression to predict the drug response for each patient and calculated the AUC for each compound, with a lower AUC suggesting increased sensitivity. Then, we evaluated the appropriate drug in terms of the difference in response and correlation analysis (Figures 7E, F). For the difference analysis, we set a strict threshold $\text{Log}_2 \text{FC} > 0.01$ (CTRP) and $\text{Log}_2 \text{FC} > 0.05$ (PRISM), respectively, to identify compounds with lower AUC values, which may act as potential clinical therapies for high-risk individuals. We employed coefficients of $r < -0.2$ (CTRP) and $r < -0.1$ (PRISM) to constrain compounds that are more closely related to the NLncS score. In Figures 7E, F, a total of six compounds from CTRP and four compounds from PRISM were finally determined (all $P < 0.05$). Further, to more deeply explain the functional links between compounds and RNA molecules as

well as disease states, we performed the CMap analysis to explore available drugs (37, 52). Surprisingly, we found that dasatinib, widely used as a first-line antineoplastic agent for leukemia, had a high negative correlation, indicating that it probably exerts therapeutic effects for high-risk score patients (Figure 7G).

Discussion

As early as 1917, Morgan and colleagues first discovered the Notch gene in mutant flies, and then the Notch signaling pathway was gradually reported (53). Notch signaling is a classical pathway for tumorigenesis and disease progression by accommodating cell proliferation and differentiation, among others (54). Multiple Notch receptors exhibit oncogenic or tumor-suppressive effects in various cells (55). Many clinical trials have also assessed the anticancer efficacy of Notch inhibitors (56). Notably, the interplay of lncRNA molecules with Notch pathway-related molecules regulates a variety of malignant phenotypes of tumors (23–25). Therefore, this study is based on the lncRNA profiles from Notch signaling and aims to establish a model with the ability to predict prognosis and immune response and assist in the screening of sensitive drugs.

The symptoms of CRC are insidious and often lead to the majority of patients presenting at an advanced stage, which contributed to an unfavorable outcome (57). Presently, with the arrival of the era of individualized treatment, the stratification and refined management system for clinical patients urgently need to be improved, and CRC patients are no exception. However, current clinical measures are immature, which is reflected in the inaccuracy of disease prognosis evaluation.

Single biomarkers are also increasingly unable to meet the needs of practical applications, and more and more attention has been paid to synthesizing multiple data types to form appropriate scoring rules (58). We developed an evaluation system consisting of six key lncRNA molecules by LASSO algorithm and Cox regression analysis to perform a risk score that can be continuously quantified in CRC patients. The model showed good prognostic evaluation ability in three public cohorts and one clinical cohort, which can accurately distinguish the high-risk group to facilitate the layer management for clinical patients. This was also initially validated in an internal cohort of 115 clinical individuals.

Consistently, how to evaluate the efficacy of ICP therapy is a problem faced by the majority of oncologists (59–61). On the one hand, “magic drugs” will bring a resurrection effect to some patients, but on the other hand, improper use is likely to cause various side effects (62). Given this, we considered whether the NLncS scoring model could reflect the difference in immune response among distinct patients. We found that there was a significant difference in the pathways enriched. The high-risk group was primarily enriched in cellular or molecular pathways involved in immune processes, including B-cell receptor,

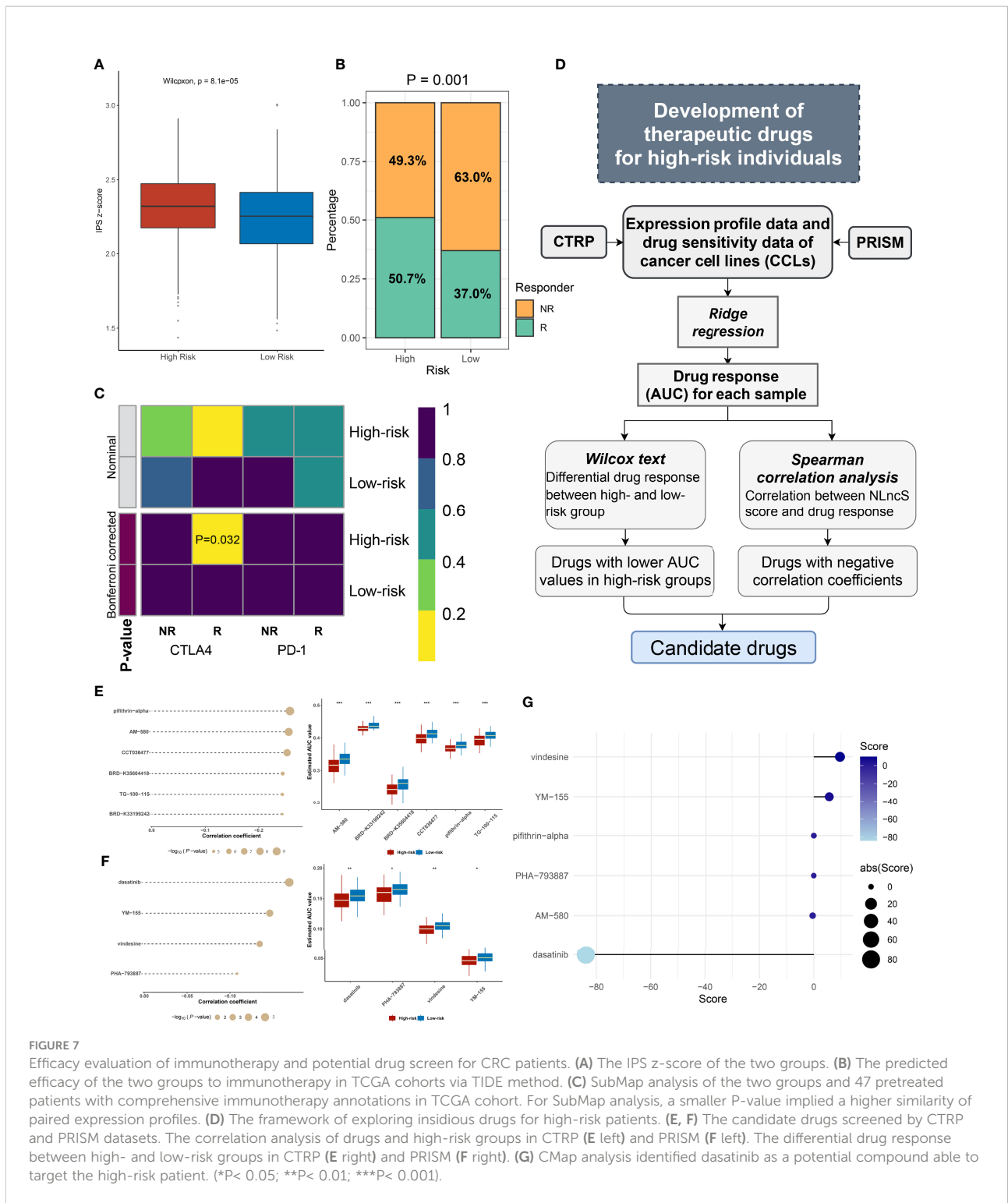


FIGURE 7 Efficacy evaluation of immunotherapy and potential drug screen for CRC patients. **(A)** The IPS z-score of the two groups. **(B)** The predicted efficacy of the two groups to immunotherapy in TCGA cohorts via TIDE method. **(C)** SubMap analysis of the two groups and 47 pretreated patients with comprehensive immunotherapy annotations in TCGA cohort. For SubMap analysis, a smaller P-value implied a higher similarity of paired expression profiles. **(D)** The framework of exploring insidious drugs for high-risk patients. **(E, F)** The candidate drugs screened by CTRP and PRISM datasets. The correlation analysis of drugs and high-risk groups in CTRP **(E** left) and PRISM **(F** left). The differential drug response between high- and low-risk groups in CTRP **(E** right) and PRISM **(F** right). **(G)** CMap analysis identified dasatinib as a potential compound able to target the high-risk patient. (* $P < 0.05$; ** $P < 0.01$; *** $P < 0.001$).

chemokine pathways, T-cell activation, and phagocytosis pathways. The low-risk group was primarily downregulated among metabolic aspects (glycolysis, TCA cycle, and oxidative phosphorylation, etc.). Further, immune landscape and immune infiltration analysis suggested visible differences and abundance.

Meanwhile, analyses of mutation and methylation levels showed that differences at the genome level were not redundant.

Growing studies have discussed two environments before immune escape occurs in the tumor: 1) ineffective infiltration of a large number of inactive T cells (63); 2) destruction of T cells

infiltrating the tumor by immunosuppressive molecules (64). Remarkably, Peng Jiang et al. raised a novel computational architecture, TIDE score, to synthesize these two environments (33). The project involved 189 studies with 33,197 specimens and was thought to be an alternative to a single predictor to analyze the efficacy of immune checkpoint suppression. As predicted, we found that the response rate to immunotherapy in high-risk (50.7%) patients was significantly better than that in low-risk (37.0%) patients ($P = 0.001$). An additional result of SubMap reported that the high-risk group appeared to be more sensitive to CTLA4-blocker-based therapy. These results validate our conjecture that the high-risk group is suitable for immunotherapy.

Dasatinib, as a first-line strategy for metastatic non-small cell lung cancer, can also be widely used as an adjuvant therapy for patients with pancreatic cancer, imatinib-resistant chronic myelogenous leukemia, etc. (65, 66). It is gratifying that we found that dasatinib is an excellent alternative drug for high-risk patients after drug sensitivity prediction and CMap analysis, which not only shows good sensitivity but also reflects powerful targeting ability. However, there is no evidence that dasatinib could be used as a first-line drug in CRC patients yet. Follow-up basic experimental and clinical studies are still needed before dasatinib is adopted to CRC patients. Nonetheless, we argued that dasatinib would possess a bright prospect in improving the prognosis of CRC patients.

Collectively, this study integrally delineated Notch-derived lncRNAs through a “NLncr” workflow and further constructed a systematic scoring system (termed “NLncS”) for accurately and stably evaluating prognosis and immune efficacy in CRC. This work may contribute to interpret patient characteristics and directed therapy. In addition, dasatinib might get a preferential seat in the first line in CRC treatment.

Data availability statement

The original contributions presented in the study are included in the article/**Supplementary Material**. Further inquiries can be directed to the corresponding authors.

Ethics statement

The studies involving human participants were reviewed and approved by Ethics Committee of The First Affiliated Hospital of Zhengzhou University. The patients/participants provided their written informed consent to participate in this study.

Author contributions

QD made the conceptualization. ZS, ZL, and YL were involved in the methodology. ZS, LL, CW, and WY provided the resources. QD, LZ, and YL analyzed the data. QD and YL

prepared the original draft. QD and WW reviewed and edited the manuscript. ZS, LL, and CW supervised the study. All authors contributed to the article and approved the submitted version.

Funding

This study was supported by The National Natural Science Foundation of China (81972663, 82173055, U2004112), The Excellent Youth Science Project of Henan Natural Science Foundation (212300410074), The Key Scientific Research Project of Henan Higher Education Institutions (20A310024), The Youth Talent Innovation Team Support Program of Zhengzhou University (32320290), The Provincial and Ministry co-constructed key projects of Henan Medical Science and Technology (SBGJ202102134), Key Scientific and Technological Research Projects of Henan Provincial Department of Science and Technology (212102310117), Henan Provincial Health Commission and Ministry of Health Co-construction Project, and Henan Provincial Health and Health Commission Joint Construction Project (LHGJ20200158).

Conflict of interest

The authors declare that the research was conducted in the absence of any commercial or financial relationships that could be construed as a potential conflict of interest.

Publisher's note

All claims expressed in this article are solely those of the authors and do not necessarily represent those of their affiliated organizations, or those of the publisher, the editors and the reviewers. Any product that may be evaluated in this article, or claim that may be made by its manufacturer, is not guaranteed or endorsed by the publisher.

Supplementary material

The Supplementary Material for this article can be found online at: <https://www.frontiersin.org/articles/10.3389/fimmu.2022.953405/full#supplementary-material>

SUPPLEMENTARY FIGURE 1

The multivariable Cox regression analysis of NLncS in GSE38832 (A). And the differences in the abundance of cell infiltrates between high- and low-risk groups (B).

SUPPLEMENTARY FIGURE 2

Correlation analysis between expression of identified methylation drivers and methylation levels.

SUPPLEMENTARY FIGURE 3

Comparison of predictive efficacy of NLncS model with three published studies.

References

- Jian X, He H, Zhu J, Zhang Q, Zheng Z, Liang X, et al. Hsa_circ_001680 affects the proliferation and migration of CRC and mediates its chemoresistance by regulating BMI1 through miR-340. *Mol Canc* (2020) 19:20. doi: 10.1186/s12943-020-1134-8
- Hernandez-Alejandro R, Ruffolo LI, Sasaki K, Tomiyama K, Orloff MS, Pineda-Solis K, et al. Recipient and donor outcomes after living-donor liver transplant for unresectable colorectal liver metastases. *JAMA Surg* (2022) 157:524–30. doi: 10.1001/jamasurg.2022.0300
- Dekker E, Tanis PJ, Vleugels JLA, Kasi PM, Wallace MB. Colorectal cancer. *Lancet* (2019) 394:1467–80. doi: 10.1016/S0140-6736(19)32319-0
- Liao T-T, Lin C-C, Jiang J-K, Yang S-H, Teng H-W, Yang M-H. Harnessing stemness and PD-L1 expression by AT-rich interaction domain-containing protein 3B in colorectal cancer. *Theranostics* (2020) 10:6095–112. doi: 10.7150/thno.44147
- Luke JJ, Lemons JM, Karrison TG, Pitroda SP, Melotek JM, Zha Y, et al. Safety and clinical activity of pembrolizumab and multisite stereotactic body radiotherapy in patients with advanced solid tumors. *J Clin Oncol* (2018) 36:1611–8. doi: 10.1200/JCO.2017.76.2229
- Fang H, Guo Z, Chen J, Lin L, Hu Y, Li Y, et al. Combination of epigenetic regulation with gene therapy-mediated immune checkpoint blockade induces antitumor effects and immune response *in vivo*. *Nat Commun* (2021) 12:6742. doi: 10.1038/s41467-021-27078-x
- Roh W, Chen P-L, Reuben A, Spencer CN, Prieto PA, Miller JP, et al. Integrated molecular analysis of tumor biopsies on sequential CTLA-4 and PD-1 blockade reveals markers of response and resistance. *Sci Transl Med* (2017) 9:eah3560. doi: 10.1126/scitranslmed.aah3560
- Zhang C, Zeng Z, Cui D, He S, Jiang Y, Li J, et al. Semiconducting polymer nano-PROTACs for activatable photo-immunometabolic cancer therapy. *Nat Commun* (2021) 12:2934. doi: 10.1038/s41467-021-23194-w
- Zhou B, Lin W, Long Y, Yang Y, Zhang H, Wu K, et al. Notch signaling pathway: architecture, disease, and therapeutics. *Signal Transduct Target Ther* (2022) 7:95. doi: 10.1038/s41392-022-00934-y
- Varga J, Nicolas A, Petrocelli V, Pestic M, Mahmoud A, Michels BE, et al. AKT-dependent NOTCH3 activation drives tumor progression in a model of mesenchymal colorectal cancer. *J Exp Med* (2020) 217:e20191515. doi: 10.1084/jem.20191515
- Wieland E, Rodriguez-Vita J, Liebler SS, Mogler C, Moll I, Herberich SE, et al. Endothelial Notch1 activity facilitates metastasis. *Cancer Cell* (2017) 31:355–67. doi: 10.1016/j.ccell.2017.01.007
- Jiang N, Zou C, Zhu Y, Luo Y, Chen L, Lei Y, et al. HIF-1 α -regulated miR-1275 maintains stem cell-like phenotypes and promotes the progression of LUAD by simultaneously activating wnt/ β -catenin and notch signaling. *Theranostics* (2020) 10:2553–70. doi: 10.7150/thno.41120
- Ciofani M, Zúñiga-Pflücker JC. Notch promotes survival of pre-T cells at the beta-selection checkpoint by regulating cellular metabolism. *Nat Immunol* (2005) 6:881–8. doi: 10.1038/ni1234
- Meurette O, Stylianou S, Rock R, Collu GM, Gilmore AP, Brennan K. Notch activation induces akt signaling via an autocrine loop to prevent apoptosis in breast epithelial cells. *Cancer Res* (2009) 69:5015–22. doi: 10.1158/0008-5472.CAN-08-3478
- Dufraigne J, Funahashi Y, Kitajewski J. Notch signaling regulates tumor angiogenesis by diverse mechanisms. *Oncogene* (2008) 27:5132–7. doi: 10.1038/onc.2008.227
- Krishna BM, Jana S, Singhal J, Horne D, Awasthi S, Salgia R, et al. Notch signaling in breast cancer: From pathway analysis to therapy. *Cancer Lett* (2019) 461:123–31. doi: 10.1016/j.canlet.2019.07.012
- Wang L, Yu S, Chan ER, Chen K-Y, Liu C, Che D, et al. Notch-regulated dendritic cells restrain inflammation-associated colorectal carcinogenesis. *Cancer Immunol Res* (2021) 9:348–61. doi: 10.1158/2326-6066.CIR-20-0428
- Maekawa Y, Ishifune C, Tsukumo S-i, Hozumi K, Yagita H, Yasutomo K. Notch controls the survival of memory CD4+ T cells by regulating glucose uptake. *Nat Med* (2015) 21:55–61. doi: 10.1038/nm.3758
- Prensner JR, Chinnaiyan AM. The emergence of lncRNAs in cancer biology. *Cancer Discov* (2011) 1:391–407. doi: 10.1158/2159-8290.CD-11-0209
- Yang X, Zhang S, He C, Xue P, Zhang L, He Z, et al. METTL14 suppresses proliferation and metastasis of colorectal cancer by down-regulating oncogenic long non-coding RNA XIST. *Mol Canc* (2020) 19:46. doi: 10.1186/s12943-020-1146-4
- Han M, Wang S, Fritah S, Wang X, Zhou W, Yang N, et al. Interfering with long non-coding RNA MIR22HG processing inhibits glioblastoma progression through suppression of wnt/ β -catenin signalling. *Brain* (2020) 143:512–30. doi: 10.1093/brain/awz406
- Qin G, Tu X, Li H, Cao P, Chen X, Song J, et al. Long noncoding RNA p53-stabilizing and activating RNA promotes p53 signaling by inhibiting heterogeneous nuclear ribonucleoprotein K deSUMOylation and suppresses hepatocellular carcinoma. *Hepatology* (2020) 71:112–29. doi: 10.1002/hep.30793
- Tao S, Chen Q, Lin C, Dong H. Linc00514 promotes breast cancer metastasis and M2 polarization of tumor-associated macrophages via Jagged1-mediated notch signaling pathway. *J Exp Clin Cancer Res* (2020) 39:191. doi: 10.1186/s13046-020-01676-x
- Hu G, Ma J, Zhang J, Chen Y, Liu H, Huang Y, et al. Hypoxia-induced lncHILAR promotes renal cancer metastasis via ceRNA for the miR-613/206/1-1-3p/Jagged-1/Notch/CXCR4 signaling pathway. *Mol Ther* (2021) 29:2979–94. doi: 10.1016/j.ymlthe.2021.05.020
- Mao X, Ji T, Liu A, Weng Y. ELK4-mediated lncRNA SNHG22 promotes gastric cancer progression through interacting with EZH2 and regulating miR-200c-3p/Notch1 axis. *Cell Death Dis* (2021) 12:957. doi: 10.1038/s41419-021-04228-z
- Jiang H, Wong WH. SeqMap: mapping massive amount of oligonucleotides to the genome. *Bioinformatics* (2008) 24:2395–6. doi: 10.1093/bioinformatics/btn429
- Liu Z, Lu T, Wang Y, Jiao D, Li Z, Wang L, et al. Establishment and experimental validation of an immune miRNA signature for assessing prognosis and immune landscape of patients with colorectal cancer. *J Cell Mol Med* (2021) 25:6874–86. doi: 10.1111/jcmm.16696
- Li Y, Jiang T, Zhou W, Li J, Li X, Wang Q, et al. Pan-cancer characterization of immune-related lncRNAs identifies potential oncogenic biomarkers. *Nat Commun* (2020) 11:1000. doi: 10.1038/s41467-020-14802-2
- Tibshirani R. The lasso method for variable selection in the cox model. *Stat Med* (1997) 16:385–95. doi: 10.1002/(sici)1097-0258(19970228)16:4<385::aid-sim380>3.0.co;2-3
- Subramanian A, Tamayo P, Mootha VK, Mukherjee S, Ebert BL, Gillette MA, et al. Gene set enrichment analysis: a knowledge-based approach for interpreting genome-wide expression profiles. *Proc Natl Acad Sci USA* (2005) 102:15545–50. doi: 10.1073/pnas.0506580102
- Liu Z, Lu T, Li J, Wang L, Xu K, Dang Q, et al. Clinical significance and inflammatory landscape of a novel recurrence-associated immune signature in stage II/III colorectal cancer. *Front Immunol* (2021) 12:702594. doi: 10.3389/fimmu.2021.702594
- Jung H, Kim HS, Kim JY, Sun J-M, Ahn JS, Ahn M-J, et al. DNA Methylation loss promotes immune evasion of tumours with high mutation and copy number load. *Nat Commun* (2019) 10:4278. doi: 10.1038/s41467-019-12159-9
- Jiang P, Gu S, Pan D, Fu J, Sahu A, Hu X, et al. Signatures of T cell dysfunction and exclusion predict cancer immunotherapy response. *Nat Med* (2018) 24:1550–8. doi: 10.1038/s41591-018-0136-1
- Charoentong P, Finotello F, Angelova M, Mayer C, Efremova M, Rieder D, et al. Pan-cancer immunogenomic analyses reveal genotype-immunophenotype relationships and predictors of response to checkpoint blockade. *Cell Rep* (2017) 18:248–62. doi: 10.1016/j.celrep.2016.12.019
- Hoshida Y, Brunet J-P, Tamayo P, Golub TR, Mesirov JP. Subclass mapping: identifying common subtypes in independent disease data sets. *PLoS One* (2007) 2:e1195. doi: 10.1371/journal.pone.0001195
- Yang Z, Yan G, Zheng L, Gu W, Liu F, Chen W, et al. As a potential predictor of prognosis and immunotherapy response for oral squamous cell carcinoma, is related to cell invasion, metastasis, and CD8+ T cell infiltration. *Oncotarget* (2021) 10:1938890. doi: 10.1080/2162402X.2021.1938890
- Lamb J, Crawford ED, Peck D, Modell JW, Blat IC, Wrobel MJ, et al. The connectivity map: using gene-expression signatures to connect small molecules, genes, and disease. *Science* (2006) 313:1929–35. doi: 10.1126/science.1132939
- Guinney J, Dienstmann R, Wang X, de Reyniès A, Schlicker A, Soneson C, et al. The consensus molecular subtypes of colorectal cancer. *Nat Med* (2015) 21:1350–6. doi: 10.1038/nm.3967
- Liu Z, Weng S, Xu H, Wang L, Liu L, Zhang Y, et al. Computational recognition and clinical verification of TGF- β -Derived miRNA signature with potential implications in prognosis and immunotherapy of intrahepatic cholangiocarcinoma. *Front Oncol* (2021) 11:757919. doi: 10.3389/fonc.2021.757919
- Liu Z, Liu L, Weng S, Guo C, Dang Q, Xu H, et al. Machine learning-based integration develops an immune-derived lncRNA signature for improving outcomes in colorectal cancer. *Nat Commun* (2022) 13:816. doi: 10.1038/s41467-022-28421-6
- Huang R, Zhou L, Chi Y, Wu H, Shi L. LncRNA profile study reveals a seven-lncRNA signature predicts the prognosis of patients with colorectal cancer. *Biomark Res* (2020) 8:8. doi: 10.1186/s40364-020-00187-3
- Zhang Z, Liu Q, Wang P, Li J, He T, Ouyang Y, et al. Development and internal validation of a nine-lncRNA prognostic signature for prediction of overall survival in colorectal cancer patients. *PeerJ* (2018) 6:e6061. doi: 10.7717/peerj.6061

43. Zeng J-H, Liang L, He R-Q, Tang R-X, Cai X-Y, Chen J-Q, et al. Comprehensive investigation of a novel differentially expressed lncRNA expression profile signature to assess the survival of patients with colorectal adenocarcinoma. *Oncotarget* (2017) 8:16811–28. doi: 10.18632/oncotarget.15161
44. Rizvi NA, Hellmann MD, Snyder A, Kvistborg P, Makarov V, Havel JJ, et al. Cancer immunology. mutational landscape determines sensitivity to PD-1 blockade in non-small cell lung cancer. *Science* (2015) 348:124–8. doi: 10.1126/science.aaa1348
45. Schumacher TN, Schreiber RD. Neoantigens in cancer immunotherapy. *Science* (2015) 348:69–74. doi: 10.1126/science.aaa4971
46. Gubin MM, Schreiber RD. CANCER. the odds of immunotherapy success. *Science* (2015) 350:158–9. doi: 10.1126/science.aad4140
47. Van Allen EM, Miao D, Schilling B, Shukla SA, Blank C, Zimmer L, et al. Genomic correlates of response to CTLA-4 blockade in metastatic melanoma. *Science* (2015) 350:207–11. doi: 10.1126/science.aad0095
48. Ma S, Chen C, Ji X, Liu J, Zhou Q, Wang G, et al. The interplay between m6A RNA methylation and noncoding RNA in cancer. *J Hematol Oncol* (2019) 12:121. doi: 10.1186/s13045-019-0805-7
49. Dang Q, Shao B, Zhou Q, Chen C, Guo Y, Wang G, et al. RNA-methyladenosine in cancer metastasis: Roles, mechanisms, and applications. *Front Oncol* (2021) 11:681781. doi: 10.3389/fonc.2021.681781
50. Nam G-H, Lee EJ, Kim YK, Hong Y, Choi Y, Ryu M-J, et al. Combined rho-kinase inhibition and immunogenic cell death triggers and propagates immunity against cancer. *Nat Commun* (2018) 9:2165. doi: 10.1038/s41467-018-04607-9
51. Yang C, Huang X, Li Y, Chen J, Lv Y, Dai S. Prognosis and personalized treatment prediction in TP53-mutant hepatocellular carcinoma: An *in silico* strategy towards precision oncology. *Brief Bioinform* (2021) 22:bbaa164. doi: 10.1093/bib/bbaa164
52. Subramanian A, Narayan R, Corsello SM, Peck DD, Natoli TE, Lu X, et al. A next generation connectivity map: L1000 platform and the first 1,000,000 profiles. *Cell* (2017) 171:1437–52. doi: 10.1016/j.cell.2017.10.049
53. Lino MM, Merlo A, Boulay JL. Notch signaling in glioblastoma: a developmental drug target? *BMC Med* (2010) 8:72. doi: 10.1186/1741-7015-8-72
54. Takebe N, Harris PJ, Warren RQ, Ivy SP. Targeting cancer stem cells by inhibiting wnt, notch, and hedgehog pathways. *Nat Rev Clin Oncol* (2011) 8:97–106. doi: 10.1038/nrclinonc.2010.196
55. Huang T, Zhou Y, Cheng AS, Yu J, To KF, Kang W. NOTCH receptors in gastric and other gastrointestinal cancers: oncogenes or tumor suppressors? *Mol Canc* (2016) 15:80. doi: 10.1186/s12943-016-0566-7
56. Chiang MY, Wang Q, Gormley AC, Stein SJ, Xu L, Shestova O, et al. High selective pressure for Notch1 mutations that induce myc in T-cell acute lymphoblastic leukemia. *Blood* (2016) 128:2229–40. doi: 10.1182/blood-2016-01-692855
57. Costea T, Hudita A, Ciolac OA, Galateanu B, Ginghina O, Costache M, et al. Chemoprevention of colorectal cancer by dietary compounds. *Int J Mol Sci* (2018) 19:3787. doi: 10.3390/ijms19123787
58. Wade JH, Alsop AT, Vertin NR, Yang H, Johnson MD, Bailey RC. Rapid, multiplexed phosphoprotein profiling using silicon photonic sensor arrays. *ACS Cent Sci* (2015) 1:374–82. doi: 10.1021/acscentsci.5b00250
59. Lin A, Qi C, Wei T, Li M, Cheng Q, Liu Z, et al. CAMOIP: a web server for comprehensive analysis on multi-omics of immunotherapy in pan-cancer. *Brief Bioinform* (2022) 23. doi: 10.1093/bib/bbac129
60. Li X, Dai Z, Wu X, Zhang N, Zhang H, Wang Z, et al. The comprehensive analysis identified an autophagy signature for the prognosis and the immunotherapy efficiency prediction in lung adenocarcinoma. *Front Immunol* (2022) 13:749241. doi: 10.3389/fimmu.2022.749241
61. Zhang J, Wang Z, Zhang X, Dai Z, Zhi-Peng W, Yu J, et al. Large-Scale single-cell and bulk sequencing analyses reveal the prognostic value and immune aspects of CD147 in pan-cancer. *Front Immunol* (2022) 13:810471. doi: 10.3389/fimmu.2022.810471
62. Georgantzoglou N, Kokkali S, Tsourouflis G, Theocharis S. Tumor microenvironment in adrenocortical carcinoma: Barrier to immunotherapy success? *Cancers (Basel)* (2021) 13:1798. doi: 10.3390/cancers13081798
63. Dunn GP, Bruce AT, Ikeda H, Old LJ, Schreiber RD. Cancer immunoeediting: From immunosurveillance to tumor escape. *Nat Immunol* (2002) 3:991–8. doi: 10.1038/ni1102-991
64. Hu-Lieskovan S, Robert L, Homet Moreno B, Ribas A. Combining targeted therapy with immunotherapy in BRAF-mutant melanoma: Promise and challenges. *J Clin Oncol* (2014) 32:2248–54. doi: 10.1200/JCO.2013.52.1377
65. Johnson FM, Bekele BN, Feng L, Wistuba I, Tang XM, Tran HT, et al. Phase II study of dasatinib in patients with advanced non-small-cell lung cancer. *J Clin Oncol* (2010) 28:4609–15. doi: 10.1200/JCO.2010.30.5474
66. Bartscht T, Rosien B, Rades D, Kaufmann R, Biersack H, Lehnert H, et al. Dasatinib blocks transcriptional and promigratory responses to transforming growth factor-beta in pancreatic adenocarcinoma cells through inhibition of smad signalling: implications for *in vivo* mode of action. *Mol Canc* (2015) 14:199. doi: 10.1186/s12943-015-0468-0